Energy 57 (2013) 295–307

Contents lists available at SciVerse ScienceDirect

Energy

journal homepage: www.elsevier.com/locate/energy

Efficiency of a new Triangle Cycle with flash evaporation in a piston engine

Michael Steffen [a,b,*], Michael Löffler [b], Karlheinz Schaber [a]

[a] Institute of Technical Thermodynamics and Refrigeration, Karlsruhe Institute of Technology, Engler-Bunte-Ring 21, 76131 Karlsruhe, Germany
[b] European Institute for Energy Research, Emmy-Noether-Strasse 11, 76131 Karlsruhe, Germany

ARTICLE INFO

Article history:
Received 27 June 2012
Received in revised form
25 November 2012
Accepted 26 November 2012
Available online 28 June 2013

Keywords:
Triangle Cycle
Organic Rankine Cycle
Isentropic efficiency
Exergetic efficiency
Flash evaporation
Cyclone

ABSTRACT

A Triangle Cycle with a piston engine expansion unit is used to convert low temperature heat into electrical energy. In this process, the isentropic efficiency of the expansion unit is considered to be unknown, and a theoretical approach for the calculation of isentropic efficiency is presented. A number of influences are taken into account – dead volume, residual mass, liquid injection performance and wall heat transfer. Various working fluids are investigated in a wide range of temperatures (333K–573K), engine speeds (5 Hz–30 Hz) and stroke volumes (0.1 L–50 L). The isentropic efficiency of water as working fluid is in the range of 0.75–0.88 and drops significantly for high stroke volumes and engine speeds. In general, injection mass has the most impact on isentropic efficiency because it influences dead volume and injection performance. The injection mass increases with vapor density and therefore is significantly influenced by working fluid and temperatures. The Triangle Cycle is compared with Organic Rankine Cycles by using determined isentropic efficiency. The exergetic efficiency of the Triangle Cycle using water is up to 35–70% higher than that of supercritical Organic Rankine Cycles in situations with a heat source temperature of up to 450K.

1. Introduction

The efficient conversion of low temperature heat and the use of waste heat for energy generation is becoming increasingly important as our global markets become even more competitive and raw materials become even more scarce [1]. Ever-increasing energy costs and complex emissions regulation leave little doubt that there is a real need to develop technologies for energy conversion. There are three different processes known for the conversion of low temperature and waste heat to energy: the Organic Rankine Cycle [2], the Kalina Cycle [3] and the Triangle, or Trilateral, Cycle [5]. Tchanche [2] and Fischer [4] present a recent collection of references.

The Organic Rankine Cycle (ORC) is similar to the well-known Clausius Rankine Cycle but employs organic working fluid instead of water. Lai et al. [6] and Saleh et al. [7] present calculations for different Organic Rankine Cycle working fluids for high-temperature and low-temperature ranges. Classical Organic Rankine Cycles are subcritical. During evaporation there is a gap between the isobaric line of the working fluid and the heat source. To avoid this concomitant exergy loss in the evaporator, supercritical ORCs are considered [6,8]. Additionally, to improve the exergetic efficiency of the evaporator and the condenser, the mixing of different working fluids for supercritical Rankine Cycles was investigated [9].

In the Kalina Cycle, a mixture of water and ammonia is used as the working fluid to improve the exergetic efficiency of evaporator and condenser. Ogriseck has investigated the influence of different ammonia contents on cycle efficiency [10].

Zamfirescu and Dincer [11] considered the use of a screw engine instead of a turbine in order to expand a mixture of ammonia and water. Screw engines allow wet vapor expansion and, therefore, the mixture can be expanded directly at boiling point. This improvement to cycle efficiency, in comparison to ORC and Kalina Cycles, is investigated theoretically with an assumed isentropic efficiency of 0.7 for the expansion unit. Zamfirescu and Dincer calculated the exergetic efficiency of their Triangle Flash Cycle to be twice that of their ORCs for the given temperature.

Kliem [12] investigated the two-phase screw-type engine using only water as the working fluid. He determined the isentropic efficiency of the expansion unit experimentally to be in the order of 0.3–0.55, depending on inlet temperature. However, due to problems with the filling process [13] and the non-adiabatic conditions

* Corresponding author. Institute of Technical Thermodynamics and Refrigeration, Karlsruhe Institute of Technology, Engler-Bunte-Ring 21, 76131 Karlsruhe, Germany. Tel.: +49 (0) 721 608 42730; fax: +49 (0) 721 608 42335.
E-mail address: michael.steffen@kit.edu (M. Steffen).

0360-5442/$ – see front matter © 2013 Elsevier Ltd. All rights reserved.
http://dx.doi.org/10.1016/j.energy.2012.11.054

Nomenclature

A	area [m^2]
a	acceleration [m/s^2]
CRC	Clausius Rankine Cycle
d	diameter [m]
EHE	external heat exchanger
$\dot{E}x$	exergy flow [J/s]
f	engine speed [1/s]
h	specific enthalpy [J/kg]
h_L	initial liquid level [m]
h_V	valve lift [m]
h_Z	cyclone height [m]
$\Delta\dot{H}$	enthalpy difference flow [J/s]
L	work [J]
$l_{E,\mathrm{ideal}}$	ideal specific work of the expansion unit [J/kg]
M	mass [kg]
$\dot{M}$	mass flow [kg/s]
N_E	number of cylinders [−]
Nu	Nusselt number [−]
ORC	Organic Rankine Cycle
p	pressure [Pa]
P	power [W]
PEEK	polyetheretherketone
Pr	Prandtl number [−]
PTFE	polytetrafluoroethylene
$\dot{Q}$	heat flow [W]
r	crank radius [m]
Re	Reynolds number [−]
S	entropy [J/K]
s	specific entropy [J/(kg K)]
$\dot{S}$	entropy flow [J/(sK)]
SS	stainless steel
T	temperature [K]
t	time [s]
t_E	injection end time [s]
t_S	injection start time [s]
TC	Triangle Cycle
v	velocity [m/s]
V	volume [m^3]
x	vapor quality [−]
X_P	penetration depth [m]
x_P	piston position [m]

Greek symbols

α	heat transfer coefficient [$W/(m^2\ K)$]
β	valve seat angle [degree]
δ	dead volume ratio [−]
ε	injection pipe diameter to valve lift ratio [−]
Φ_L	liquid level ratio [−]
γ	valve opening velocity [m/s]
η_{Ex}	exergetic efficiency [−]
η_{SE}	isentropic expansion unit efficiency [−]
η_{SP}	isentropic pump efficiency [−]
η_{th}	thermal efficiency [−]
φ	crankshaft angle [rad]
κ	thermal diffusivity [m^2/s]
λ	drag coefficient [−]
λ_S	stroke-connection rod ratio [−]
μ	residual mass ratio [−]
ν	kinematic viscosity [m^2/s]
θ	valve timing ratio [−]
ρ	density [kg/m^3]
τ	dimensionless time [−]
ζ	cyclone diameter to injection pipe diameter ratio [−]
Δ	Triangle Cycle
$\square$	ORC

Subscripts

$'$	state point at saturated liquid line
$''$	state point at saturated vapor line
$*$	ideal state point
1,2,3,4,5,6	state points
c	centrifugal
crit.	critical state point
d	dead
diss	dissipation
E	end
h	hydraulic
HC	heat carrier
I	injection
irr	irreversible
in	inlet
L	liquid
max	maximum
min	minimum
out	outlet
P	piston
R	residual
S	stroke
T	total
U	ambient state
V	vapor
W	wall-surface
WF	working fluid
Z	cyclone

within the screw engine, the isentropic efficiency of this engine is too low to compete with the ORC and Kalina Cycles.

Fischer [4], Bombarda [3] and Zamfirescu [11] compared the exergetic efficiency of the different cycles. Fischer [4] compared a Triangle Cycle (using water as the working fluid) with ORCs (using different working fluids) and found that the "exergetic efficiency for power production is larger by 14%–29% for the Triangle Cycle than for the ORC". Bombarda [3] presented a comparison between the Kalina Cycle and the ORC with the result that both cycles have almost the same net power output (for a heat source at 619 K). Fischer [4], Bombarda [3] and Zamfirescu [11] determined that a reliable comparison of these cycles is only valid if the entire process is taken into account, including external heat exchanger, condenser and expansion unit with their respective exergy losses.

Isentropic efficiency is the dominant factor in exergy losses in the expansion unit. High values of isentropic efficiency are often considered when looking at turbines, however, it should be noted, that these are only valid for big scale engines and optimized operating points. Reliable isentropic efficiencies for the Triangle Cycle have not been fully explored, and are almost unknown in literature.

This paper investigates the isentropic efficiency of the expansion unit used in the Triangle Cycle. First, the Triangle Cycle is described and then the fundamentals for the process realization are presented. A model using different impacts to calculate isentropic efficiency is then presented. Finally, the Triangle Cycle is compared to ORCs using different working fluids and heat source temperatures.

2. Description of the ideal Triangle Cycle

The flow diagram of the Triangle Cycle is shown in Fig. 1, which illustrates eight state points. Fig. 2 shows the *T*–*S*-diagram of the ideal Triangle Cycle in which water is the working fluid. In the pump, the pressure of the saturated liquid (state point 1) is increased to the saturation pressure of the temperature at point 3 (state point 2). After this, the subcooled liquid enters the heater where the temperature increases to the saturation temperature of the prevailing pressure (state point 3). Afterwards, the liquid is injected into the expansion unit and expands to the condensation pressure into the two phase region (state point 4). Finally, the two phase flow is totally liquefied in the condenser.

In the external heat exchanger (EHE) a sensible heat source is used to heat up the working fluid. At that point, the heat carrier cools down from the inlet temperature (state point 5) to the outlet temperature (state point 6). Within the condenser, the coolant is heated up from the inlet temperature (state point 7) to the outlet temperature (state point 8) in order to condense the working fluid.

During the expansion step (from state point 3 to state point 4) a certain amount of vapor is generated while the heat of evaporation is supplied by the liquid, which then cools down. In comparison to turbine processes (for example CRC, ORC and Kalina Cycles) evaporation and expansion takes place simultaneously in the same unit. The greatest advantage of the Triangle Cycle is a significant reduction in exergy loss due to using a liquid–liquid heat exchanger instead of an evaporator. Hence, the Triangle Cycle is best suited to the isobaric line of the sensible heat source.

3. Necessary requirements for the realization of the Triangle Cycle with a piston engine expansion unit

In the Triangle Cycle described here, a piston engine is used as an expansion unit in which a certain amount of liquid is injected each time the piston reaches the top dead center. This discontinuous operation of a piston engine with flash evaporation is the principle operational difference from a continuously working turbine or screw-engine. Hence injection timing, dead volume and residual mass have to be taken into account.

In order for the Triangle Cycle to be successful there are technical requirements and boundary conditions, which must be met. These will be discussed in the following sections.

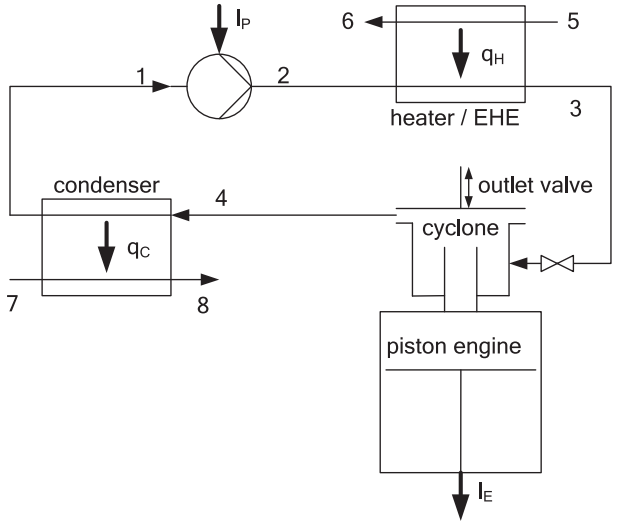

Fig. 1. Flow diagram of the Triangle Cycle.

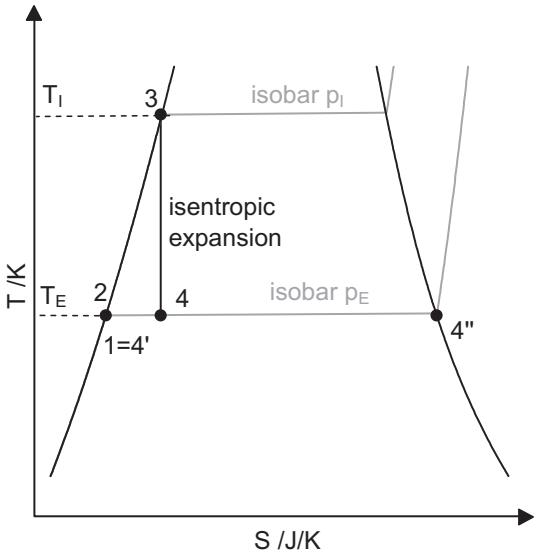

Fig. 2. *T*–*S*-diagram of the Triangle Cycle with working fluid water.

3.1. Phase separation in a cyclone

Injection and flash evaporation takes place in a small cyclone above the piston chamber which provides the phase separation of liquid and vapor. For the Triangle Cycle, it is very important for the liquid to be kept out of the piston chamber. This will avoid hydraulic shocks and heat transfer between the liquid and the piston or cylinder. The heat exchange surface between the liquid and the piston engine can be reduced by restraining the liquid in the cyclone. During flash evaporation the liquid cools down significantly from injection temperature to expansion end-temperature. Löffler [14] has given a calculation that shows a satisfactory separation curve for suitable cyclone geometry. High injection pressure and small cyclone diameter result in high injection velocity so that a huge centrifugal acceleration can be induced. This acceleration is orders of magnitude higher than the acceleration of gravity.

In contrast to this, there are two phenomena that have to be discussed according to the evaporation inside the cyclone. First, an explosive-like generation of vapor with bubble breakup and droplet entrainment has to be mentioned. Second, the large amount of vapor, mainly generated inside the liquid phase, results in a bubble flow which might be harmful for phase separation. Additionally, incomplete phase separation is probable due to high vapor velocities between the cyclone and the piston chamber. We assume a satisfactory phase separation with a reasonable minimum size of cyclone volume because it is possible to prevent liquid overspill with special built-in fitments.

3.2. Prevention of condensation in the cylinder

To prevent vapor condensation inside the piston chamber, the whole machine has to be heated up to a minimum of injection temperature. Unlike the expansion of superheated vapor, saturated vapor will condense directly on any colder surface and is accompanied by an unwanted liquid mass transport in the direction of the piston chamber.

If the liquid enters the piston chamber, the evaporating liquid cools the cylinder surface significantly. Consequently, it is difficult to maintain the surface temperature, and it is even more difficult to evaporate all the liquid by thermal heat input. Added to this, remaining liquid within the piston chamber cools down during

expansion and can act as a cold surface causing condensation of vapor during the following injections. This again underlines the necessity of preventing the liquid from flooding the cylinder by using a cyclone for phase separation. If only vapor enters the piston chamber, the amount of heat needed to maintain the temperature of the cylinder wall is small because of the small heat transfer coefficient. The input of thermal heat then is in the scale of 5% [15]. This value is related to a heat transfer between vapor and cylinder wall for a mean vapor velocity of 20 m/s and water as working fluid, which is expanded from 573K to 373K (heat losses of the expansion unit are considered and are included in this value).

3.3. Thermal insulation of cyclone surface

Inside the cyclone, the injected liquid rotates on a tight circular path at a high velocity to ensure satisfactory phase separation. This leads to high Reynolds-numbers and remarkable heat transfer conditions. But, in order to attain a highly efficient process, the conditions should be adiabatic because heat transfer between the liquid and cyclone wall causes exergy losses. More precisely, there is a transient heat transfer problem [15]. The injected hot liquid cools down rapidly during expansion and displacement of the piston within the first half of a cycle (top dead center to bottom dead center). During the second half of a cycle (bottom dead center to top dead center) the now-cooled liquid still rotates inside the cyclone until it is discharged. When liquid temperature is higher than surface temperature, heat is transferred from the liquid to the cyclone wall. This amount of heat is initially lost for energy conversion but is regained later in the cycle. When liquid temperature falls below wall temperature almost the same amount of heat is transferred back to the liquid phase. This reverse heat transfer takes place at lower temperature and at lower exergetic efficiency and leads to exergy loss. Moreover, the piston then moves from bottom dead center to top dead center and any increase of temperature (equivalent to an increase of pressure) leads to greater effort to discharge the working fluid.

This kind of oscillating transient heat exchange problem can be resolved by using a thermal insulating layer to significantly minimize the heat that is transferred between the liquid and the wall, and thus to minimize exergy loss. It is possible to calculate the depth of penetration of the temperature wave into the wall (see Section 4.2.8).

3.4. Fast liquid injection valve

The heat of evaporation is provided by the sensible heat of the cooling liquid. To maintain this heat, a large input of liquid mass is needed to generate a certain amount of vapor. The quantity of injection mass depends on the temperature range, the working fluid and the stroke volume. In order to obtain a highly efficient process, a quick injection of liquid mass is required.

At best, the injection should take place near top dead center after the outlet valve is closed. After the piston is displaced, flashing of the liquid starts and the liquid cools down. Any further injection of hot liquid leads to mixing hot and cooled liquid, which results in exergy loss.

3.5. Vapor and liquid outlet valve

The flow cross sectional area of the outlet valve has to be dimensioned sufficiently to prevent compression of the vapor during discharge and to ensure that the working fluid is completely discharged. Any residue of working fluid after one cycle leads to accumulation and flooding of the cyclone. The outlet valve needs to be open during almost the complete second half of one cycle, when the piston moves from bottom to top dead center. Therefore, it is necessary to have precise and rapid valve control. Timing for closing the outlet valve is particularly important to ensure sealing prior to injection. This ensures that cycle efficiency is not reduced by a bypass of inlet and outlet.

4. Modeling of the expansion engine

A piston engine is used to realize the Triangle Cycle. The following section addresses the simulation of the isentropic efficiency of the piston engine.

The expansion engine must perform with the technical components (cyclone, inlet and outlet valves and cylinder wall heating) and perform in working conditions as described in Section 3. These components and working conditions can create opportunities for exergy losses through dead volume, residual mass, injection performance and heat transfers. Their impact on isentropic efficiency is specified in Section 5.

4.1. Energy balance

At first, an energy balance of the expansion unit is considered and the theoretical power output as well as the required injection mass is derived.

Equation (1) is used to calculate the mechanical power output of the expansion unit.

$$P = \eta_{SE} N_E f M_I l_{E,\mathrm{ideal}} \tag{1}$$

Besides the isentropic efficiency η_{SE}, N_E is the number of cylinders, f the engine speed, M_I the injection mass per cylinder and $l_{E,\mathrm{ideal}}$ the specific ideal work. $l_{E,\mathrm{ideal}}$ depends on the enthalpies of the state points at the inlet h_3 and outlet h_4 of the expansion unit, as well as on the vapor quality x at the end of the expansion (Equation (2)). The vapor quality is the ratio of vapor mass to total mass $x = M_V/M_T$. We assume state point 3 to be at boiling point at injection temperature $T_I = T_3$ and state point 4 to be within the two phase region at expansion end-temperature $T_E = T_4$.

$$l_{E,\mathrm{ideal}} = h_{3'} - h_4 = h_{3'} - x h_{4''} - h_{4'}(1-x) \tag{2}$$

Equation (3) gives the required injection mass M_I in dependence of the stroke volume of the piston engine V_S and the thermodynamic state at the expansion end point, namely vapor quality x, density of vapor and liquid at expansion end-temperature T_E.

$$M_I = \frac{V_S}{\frac{x}{\rho_V(T_E)} + \frac{(1-x)}{\rho_L(T_E)}} \tag{3}$$

With the assumption of an isentropic expansion, the vapor quality x is given by Equation (4).

$$x = \frac{s_{3'} - s_{4'}}{s_{4''} - s_{4'}} \tag{4}$$

The thermal efficiency η_{th} is the ratio of work output and heat input. The real state points 2 and 4 include isentropic efficiencies of the expansion unit and the pump. Alternatively, we can take the ideal state points 2* and 4* and use the isentropic efficiencies η_{SE} for the expansion unit and η_{SP} for the pump (Equation (5)). The use of thermal efficiency is most common in power plants.

$$\eta_{\mathrm{th}} = \frac{(h_3 - h_4) - (h_2 - h_1)}{(h_3 - h_2)} = \frac{\eta_{SE}(h_3 - h_{4^*}) - \eta_{SP}(h_{2^*} - h_1)}{(h_3 - h_2)} \tag{5}$$

When looking at the use of low temperature heat, the exergetic efficiency of the cycle is more useful because it gives the ratio

of how much of the available exergy is converted to work. The exergy is related to the ambient state indicated with subscript *U*.

$$\eta_{Ex} = \frac{(h_3 - h_4) - (h_2 - h_1)}{h_5 - h_U - T_U(s_5 - s_U)} \frac{\dot{M}_{WF}}{\dot{M}_{HC}} \tag{6}$$

For Equation (6) the mass flows of the working fluid and the heat carrier have to be known.

4.2. Isentropic efficiency

4.2.1. Simulation tools

MATLAB®/Simulink® by MathWorks® is used to simulate the expansion unit presented in the following chapters. Two different solvers, with fixed and variable time steps, are used. For the fixed time step, a third order accuracy solver *ode3* based on the Bogacki-Shampine Formula [18] integration technique is used with a fixed time step of 5×10^{-5} s. This solver is used if wall heat transfer is integrated into the simulation and the wall discretization is also based on fixed time step. In all other cases, the much faster variable time step solver *ode45* based on Runge-Kutta [19] is used. REFPROP [17] is included in the simulation. This empowers the calculation of a wide range of different working fluids. When showing the effects of the various impacts on the isentropic efficiency, water is taken as the working fluid of the Triangle Cycle. Section 5 presents the results for isentropic efficiency for a selection of working fluids.

4.2.2. Basic thermodynamic model

A thermodynamic model has been developed with respect to the most important impacts on the isentropic efficiency. This enables the calculation of the isentropic efficiency of the real machine power output.

Power is calculated by the well-known Equation (7).

$$P = N_E f L = N_E f \left(- \int_0^{1/f} \left(p \frac{dV_S}{dt} + \frac{dL_{diss}}{dt} \right) dt \right) \tag{7}$$

Within this equation the pressure p and the stroke volume V_S are unknown. The time derivative of the stroke volume, respectively the product of the piston velocity and the piston area, is a well-known function for piston engines [20].

Both entropy and mass balance are used to calculate the total entropy S_T and the total mass M_T. The specific entropy s is calculated by dividing the total entropy S_T by the total mass M_T within the system boundary. In the same way, the density ρ is calculated by dividing the total mass M_T by the total volume V_T, which is the sum of V_S and the dead volume V_d. Furthermore, the total mass M_T is obtained by integrating the inlet and outlet mass flow starting with the residual mass M_R that remains inside the dead volume after discharge. The inlet mass flow contains the liquid mass at injection temperature T_I and the outlet mass flow contains both the liquid and vapor mass flow at expansion end-temperature T_E.

$$\int_{M_R}^{M_T} dM = \int_0^{1/f} \left(\dot{M}_{in} - \dot{M}_{out} \right) dt \tag{8}$$

Finally the entropy S_T is calculated by an entropy balance. This takes into account the change of entropy by inlet and outlet mass flow, heat transfer, as well as the irreversible entropy flow. The entropy balance is given by Equation (9).

$$\int_{S_R}^{S_T} dS = \int_0^{1/f} \left(\frac{1}{T} \dot{Q} + s_{in} \dot{M}_{in} - s_{out} \dot{M}_{out} + \dot{S}_{irr} \right) dt \tag{9}$$

By knowing the irreversible entropy flow, the dissipated work used in Equation (7) can be calculated by using the following equation. At first we consider reversible processes where L_{diss} respectively $\dot{S}_{irr}$ are zero.

$$\frac{dL_{diss}}{dt} = T \dot{S}_{irr} \tag{10}$$

Then the pressure p is calculated as a function of entropy s and density ρ by using REFPROP [17].

In the following section, the boundary conditions and simulation results first, for the ideal machine and second, for a real machine, are shown. In the latter, dead volume, residual mass, inlet and outlet valve timing, as well as wall heat transfer are taken into account. In order to calculate the impacts of the particular effect, mechanical losses are not considered in this chapter. In Section 5 mechanical losses due to friction of the piston, rod gland and bearing are considered by a factor of 0.90 [16], which is then included into the isentropic efficiency.

4.2.3. Ideal machine

In a ideal point of view, when no dead volume (cyclone volume) is considered, the injection of liquid is linked to the movement of the piston so that, during injection, the stroke volume equals the volume of the liquid and no flash evaporation takes place (see Fig. 3: constant temperature and pressure during the injection). When injection is complete, inlet mass flow drops to zero. Flash evaporation takes place in the cylinder with a drop in pressure and temperature. This occurs during the piston movement from top dead center to bottom dead center, as can be seen in Fig. 3. From bottom dead center ($\tau = 0.5$) to top dead center ($\tau = 1$) the total mass M_T is discharged at constant pressure and temperature. The ideal outlet mass flow $\dot{M}_{out}$ is calculated by piston velocity, the piston area and the density ρ. The results for power output and volumetric work density are equal to the results gained by Equation (7), which validates the simulation on a fundamental level. Mechanical losses are not considered here.

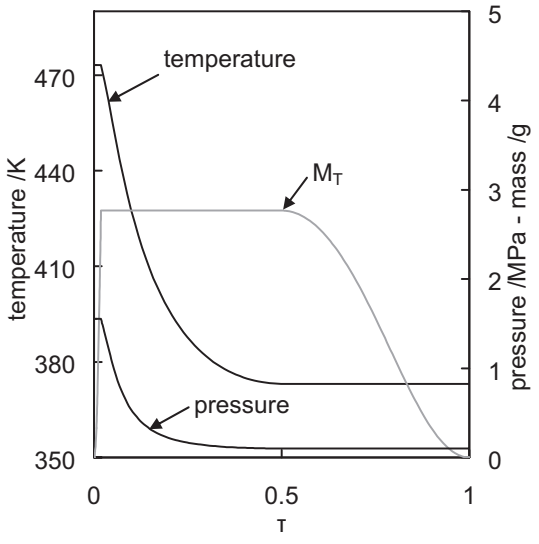

Fig. 3. Simulation results of ideal expansion unit, τ is the dimensionless cycle time, $T_I = 473.15$ K, $T_E = 373.15$ K.

4.2.4. Dead volume

As a consequence of using a cyclone, an injection pipe and valves, dead volume must be taken into account in the modeling of isentropic efficiency. In the dead volume, injected liquid evaporates suddenly, without moving the piston, and results in a loss of exergy.

The virtual absolute minimum cyclone volume equals the volume of the injected liquid mass. We consider a necessary cyclone volume (dead volume) of δ times the volume of the injection mass at injection conditions (Equation (11)). A realistic minimum value of δ is of the order of 3, caused by the necessary space and diameters for the vapor, flowing from the cyclone to the cylinder, as well as for the injection pipe. When optimizing the cyclone shape in the frame of phase separation much higher values of δ might be necessary. The value δ doesn't initially determine the shape of the cyclone.

We assume that the mass remaining within the dead volume after discharge is vapor and liquid at the vapor fraction given by Equation (4). Additional remaining liquid is discussed in Section 4.2.5.

$$\delta = \frac{V_d}{M_I/\rho_L(T_I)} \tag{11}$$

Fig. 4 shows the isentropic efficiency in dependence of the factor δ. The isentropic efficiency depends strongly on hot and cold temperature and the injection mass. With increasing vapor density at T_E, the injection mass and dead volume increases and isentropic efficiency decreases. This effect is more problematic for working fluids with higher vapor densities, and therefore higher injection masses, than water.

4.2.5. Residual liquid mass

At the beginning of one cycle, the working chamber should not contain any working fluid from a former cycle. A small amount of vapor and liquid will remain after discharge in the dead volume; this is considered in Section 4.2.4. Here we take into account that additional liquid will remain inside the expansion unit, potentially caused by ineffective alternation of load or by incomplete phase separation. Even a small amount of residual mass leads to a significant decrease in isentropic efficiency, because the residual mass, initially at expansion end-temperature T_E, has to be heated to the actual evaporation temperature. Mixing of hot injection mass with cold residual mass leads to dissipation. The ratio of residual mass and injection mass is given by the factor μ.

$$\mu = \frac{M_R}{M_I} \tag{12}$$

In addition to the thermodynamic disadvantages of residual mass inside the working chamber, there is also a potential mechanical problem because accumulating liquid inside the cylinder leads to hydraulic shocks, which may destroy the machine. Hydraulic shocks are not considered within this simulation.

The simulation results for two different dead volume ratios are given in Fig. 5. It is easy to recognize the expected significant decrease in isentropic efficiency with increasing residual liquid mass. This emphasizes the need for an efficient discharge of working fluid in each alternation of load.

4.2.6. Design rules for cyclone geometry and inlet

The shape of the cyclone and the injection pipe have to be defined in more detail before looking at valve control for injection and wall heat transfer. The objective of cyclone design rules is to find universally valid dependencies of geometric proportions which are applicable to a wide range of working fluids and injection masses. Nevertheless, for each individual case, the cyclone and inlet geometry must be optimized.

The liquid injection mass M_I has to be accelerated to the injection velocity v_I by the thrust of the liquid. Acceleration takes place in the injection pipe with diameter d_I. A valve is opened between the times t_S and t_E with the valve lift h_V. The required liquid mass has to be injected within that time period and through the given cross-section. Injection velocity needs to be at a certain level to achieve the required centrifugal acceleration. Pressure drop, wall friction and back-pressure from inside the cyclone are not taken into account.

The injection pipe diameter is calculated by Equation (13) and depends on the factor γ that represents the opening velocity of the valve ($\gamma = h_{V,\max}/\Delta t$) and ε as the ratio of injection pipe diameter and the valve lift ($\varepsilon = d_I/h_{V,\max}$).

$$d_I = \varepsilon\gamma\frac{(t_E - t_S)}{2} \tag{13}$$

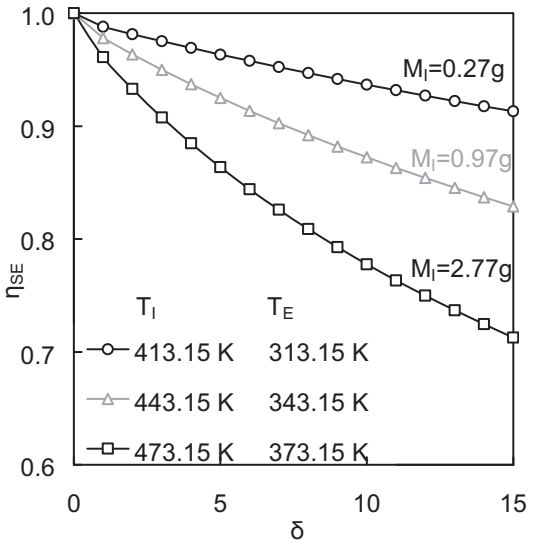

Fig. 4. Isentropic efficiency in dependence of the dead volume ratio for different temperatures and injection masses; working fluid: water.

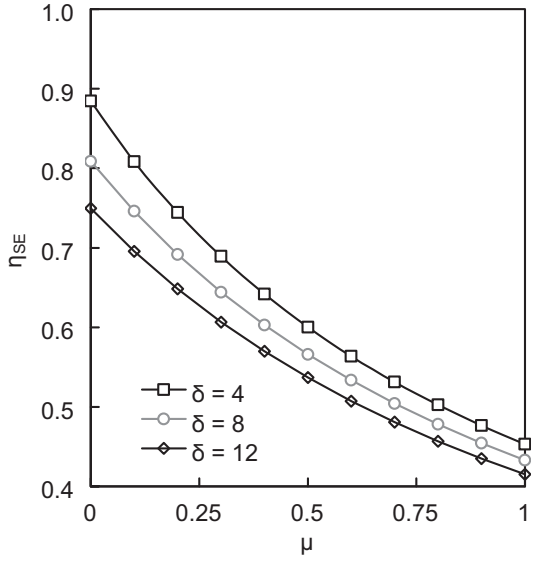

Fig. 5. Isentropic efficiency in dependence of the residual mass ratio; working fluid: water; T_I = 473.15 K, T_E = 373.15 K; M_I = 2.77 g.

We consider the valve lift to be a symmetric sine-shaped function as given by Equation (14).

$$h_V(t) = \frac{h_{V,\max}}{2}\left[\sin\left(\frac{2\pi}{t_E - t_S}t - \pi\left(\frac{t_E + t_S}{t_E - t_S} - \frac{1}{2}\right)\right) + 1\right] \quad (14)$$

The cross-sectional area is calculated as follows with the valve seat angle β:

$$A(t) = \min\left\{\frac{\pi}{4}d_I^2; \pi d_I h_V(t)\sin\beta\right\} \quad (15)$$

Using the continuity equation, the mass flow is then given by Equation (16)

$$\dot{M}_{\text{in}}(t) = \rho_L(T_I)\cdot\int\frac{p_I A(t)}{M_I}\mathrm{d}t\cdot A(t) \quad (16)$$

By integrating Equation (16) within the boundaries of t_S and t_E an injection mass is calculated that has to fit the injection mass M_I by varying the injection end time t_E. Moreover the injection velocity has to reach the velocity $v_C = \sqrt{a_C(d_Z/2)}$ whereas the cyclone diameter is given by $\zeta = d_Z/d_I$ and a_C is set to 200,000 m/s^2. A high centrifugal acceleration is required to reach a satisfactory phase separation. Even when neglecting friction or pressure drop, a minimum time period is needed to accelerate and inject a certain amount of liquid working fluid. This calculation depends on the geometric ratios γ, ε, β and ζ and on the process parameters M_I, T_H, $t_E - t_S$ and p_I. In the following section, we take a closer look at the geometric values.

For common hydrocyclones we find values for ζ of the order of 3.6–7 [21]. For constructive simplicity ζ is set to 6.

The value ε gives the ratio of the injection pipe diameter to the valve lift. With increasing ε the injection pipe diameter increases and the valve lift, as well as the injection time period, decreas. But with increasing injection pipe diameter, the cyclone diameter also increases and a higher injection pressure is needed to reach the required injection velocity and centrifugal acceleration. Within this simulation a maximum value of ε is calculated for a constant injection pressure. ε, must have the highest possible value that is equal, or less than, 3. The injection pressure is set within the simulation to the maximum of 3 MPa and the particular saturation pressure at injection temperature. This high injection pressure ensures a fast injection of the liquid without falling below saturation pressure.

The valve opening velocity γ should be as high as possible but is limited by the actuation of the valve and the valve geometry itself. Injection valves used in combustion engines reach values of γ of the order of 1 m/s. By using a crank-shaft we find a maximum velocity of 0.8 m/s [22]. With the aim of a universally valid simulation we use $\gamma = 1$ m/s.

Fig. 6 shows the injection time period $t_E - t_S$ in dependence of the required injection mass for different values of γ and ε for the conditions given by the figure caption. The corresponding injection pipe diameter can easily be calculated by Equation (13). A shorter injection time period for a constant injection mass can be obtained by increasing ε. This also results in the limitation by the required injection velocity for the given injection pressure of 3 MPa, which was mentioned previously. For high injection masses, a lower value of ε results in increasing injection time period but yields to the required injection velocity.

With increasing stroke volume of the piston engine, as well as with higher engine speed, the injection time period gains in importance. Injection mass increases with stroke volume and the time period needed for injection is prolonged in relation to engine speed. By decreasing the engine speed, higher stroke volumes are feasible. Section 5.2 takes a closer look at this topic.

Within the cyclone, the initial liquid level should be low to improve phase separation. Saury et al. [23] investigated the

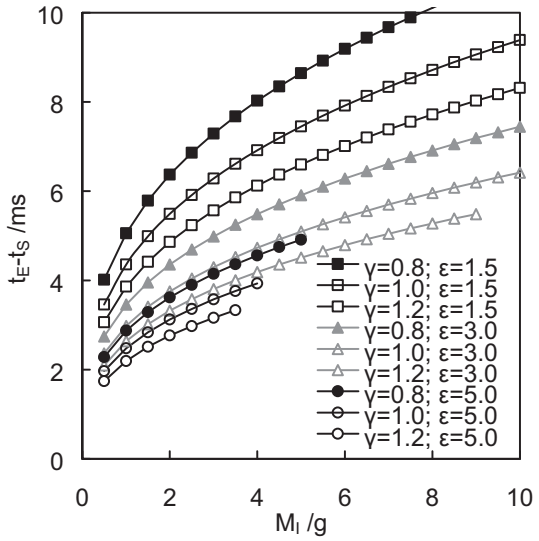

Fig. 6. Injection time period in dependence of injection mass for different values of γ and ε; $\rho_L = 1000$ kg/m^3; $\beta = 60°$; $\zeta = 6$; $a_C = 200{,}000$ m/s^2; $p_I = 3$ MPa.

maximum phenomenon amplitude (a bubble layer between liquid and vapor due to evaporation) for flash evaporation in a chamber. In these experiments negative pressure conditions are present. These experiments do not show the increased gravitation (from centrifugal acceleration) and the high depressurization rates that are present in cyclones with flash evaporation. Nevertheless, the results show rising maximum phenomenon amplitude with increasing initial water height. In the case of flash evaporation in cyclones, this maximum phenomenon amplitude could lead to cyclone flooding.

We use $\phi_L = h_L/d_I = 0.25$ as the ratio of the initial liquid level to the injection pipe diameter. Alternatively, $h_L/d_Z = 0.042$ is given by ϕ_L/ζ. Hence, the cyclone height is given by Equation (17). During evaporation the liquid level does not stay constant due to reduction of liquid phase and bubble formation within the liquid. Therefore h_L represents an initial value here.

$$h_Z = \frac{M_I/\rho_L(T_I)}{\frac{\pi}{4}\left(d_Z^2 - (d_Z - 2h_L)^2\right)} \quad (17)$$

The cyclone volume ratio δ is calculated by Equation (18) using a cylinder shaped cyclone with a cone shaped inset for the reduction of dead volume. With the given values for ζ and ϕ_L the dead volume ratio δ is 4.2. Fig. 7 shows a sketch of the mentioned cyclone geometry and geometric dimensions.

$$\delta = \frac{\zeta^2 - \frac{\zeta^2}{3}}{4\phi_L\zeta - 4\phi_L^2} \quad (18)$$

Finally, the cyclone surface for calculation of the heat exchange between working fluid and cyclone wall is determined by Equation (19). Only the lateral surface of the cylinder shaped cyclone is considered to be in contact with the liquid. For low liquid levels this simplification is justified.

$$A = \pi d_Z h_Z \quad (19)$$

4.2.7. Valve control and injection

With the help of the cyclone design parameters from Section 4.2.6, the valve timing is given as a function of the values γ and ε.

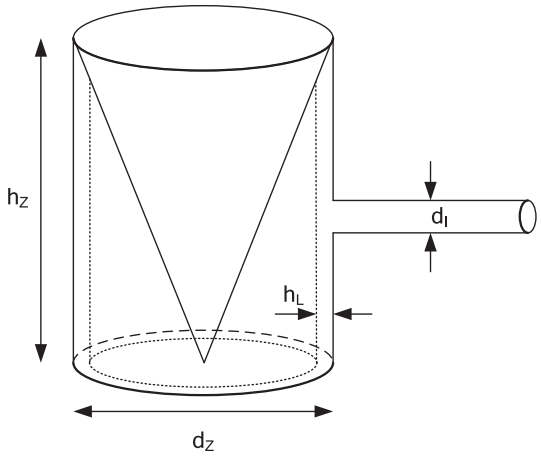

Fig. 7. Sketch of cylinder shaped cyclone with cone shaped inset.

When the injection valve is opened, the outlet valve has to be closed to ensure there is no bypass between inlet and outlet. This means, for injection start times before top dead center, the discharge of the working fluid is terminated and non-discharged working fluid is treated as residual mass.

Within this simulation the factor θ (Equation (20)) is the ratio between the opening time period and the cycle period respectively, the engine speed f.

$$\theta = (t_E - t_S)f \tag{20}$$

The factor θ_S is the ratio of injection start time and the engine speed f. A negative value of θ_S indicates that the injection start is before the piston reaches top dead center.

$$\theta_S = t_S f \tag{21}$$

Fig. 8 shows the isentropic efficiency as a function of the injection start time t_S for a number of different opening time period ratios θ. For each injection time period there is an optimum injection start time at $t_S = -0.002$ s for the given injection conditions. We found the optimum to be $\theta_S = -0.57 \cdot \theta$ by evaluating different

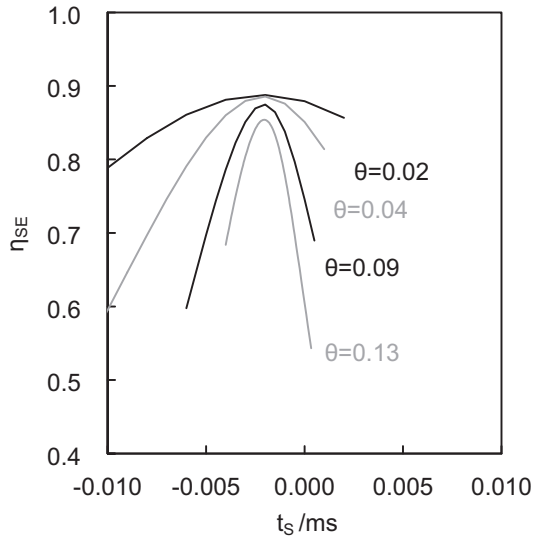

Fig. 8. Isentropic efficiency in dependence of the injection start time for different opening time period ratios; working fluid: water; $T_I = 473.15$ K, $T_E = 373.15$ K; $\delta = 4.2$.

simulation results for different working fluids and temperatures. The isentropic efficiency at optimum injection start time decreases slightly with an increasing injection time ratio (higher engine speed or longer injection time). In Section 5.2 we will have a closer look at the dependence of engine speed on isentropic efficiency.

For higher injection time periods, it is increasingly important to find the optimum injection start time in the scale of milliseconds by an appropriate valve actuation, as shown in Fig. 8.

It must be noted that, when an injection start time differs from top dead center, the injection mass has to be adapted in order to reach the same expansion end-temperature T_E. Therefore, the maximum stroke volume V_S in Equation (3) is reduced by the actual stroke volume at the time the injection starts. An injection start time before top dead centre of the piston engine yields a reduced injection mass and vice versa. An adopted injection mass has been taken into account in the calculation of the isentropic efficiency.

4.2.8. Wall heat transfer

As described in Section 3.3 a thin thermal insulating layer on the cyclone surface has to be used to minimize heat transfer between the working fluid and the cyclone wall. Nevertheless, heat transfer between the rotating working fluid inside the cyclone and the cyclone wall cannot be neglected. This chapter presents the calculation of heat flow used in Equation (9). To calculate the heat flow we use Fourier's Law with heat transfer coefficient α, heat exchange surface A and temperature difference between wall-surface temperature T_W and liquid temperature T_L. The heat exchange surface A is given by Equation (19).

$$\dot{Q} = \alpha A (T_W - T_L) \tag{22}$$

For calculation of the heat transfer coefficient α the Nu-correlation given by Equation (23) with $\xi = (1.8 \log_{10} Re - 1.5)^{-2}$ [24,25,26] is applied.

$$Nu = \frac{(\xi/8) Re\, Pr}{1 + 12.7\sqrt{\xi/8}\left(Pr^{2/3} - 1\right)} \left[1 + \left(\frac{d_h}{\pi d_Z}\right)^{2/3}\right] \tag{23}$$

The hydraulic diameter d_h is 4 times the cross sectional area divided by the perimeter of the flow profile.

The Re-number depends on the velocity v_L of the rotating fluid, the hydraulic diameter d_h and the kinematic viscosity ν.

Even though the flow regime inside the cyclone is three-dimensional and complex, the velocity of the rotating fluid v_L is calculated by a simple momentum balance given by Equation (24) with drag coefficient λ [27], inlet and outlet mass flow $\dot{M}_{\text{in}}$ and $\dot{M}_{\text{out}}$, and the liquid mass M_L.

$$\frac{\mathrm{d}v_L}{\mathrm{d}t} = -\frac{\lambda}{2} v_L^2 \frac{1}{d_h} + \frac{\dot{M}_{L,\text{in}} v_{\text{in}} - \dot{M}_{L,\text{out}} v_L - \dot{M}_L v_L}{M_L} \tag{24}$$

The inlet velocity is calculated by using Equation (16).

A one-dimensional discretization model is used to calculate the temperature profile inside the cyclone wall because the wall-surface temperature T_W depends on the transient heat conduction inside the cyclone wall [28]. We use cylindrical coordinates and a grid with variable step size. The grid resolution close to the cyclone surface is thin and this allows a good resolution for achieving the transient temperature profile.

The cyclone wall is considered to be segmented in three layers with zero resistance heat contact between them. The first layer, which is in contact with the rotating fluid, is as thick as the estimated penetration depth given by Equation (25) [29] in which the amplitude of the temperature profile is reduced to 1%. This layer has a fine-meshed grid of 10^{-5} m. The second layer has the thickness of 10^{-2} m

Table 1
Thermal properties of different cyclone wall materials.

	PTFE	PEEK	SS	Brass	Aluminum
κ/m^2/s	9.47×10^{-8}	1.41×10^{-7}	3.75×10^{-6}	3.593×10^{-5}	9.70×10^{-5}
X_P/m (at 10 Hz)	0.253×10^{-3}	0.313×10^{-3}	1.592×10^{-3}	4.925×10^{-3}	8.093×10^{-3}

minus the thickness of the first layer and the third layer has a thickness of 10^{-2} m. Both the second and third layers have a coarser grid to reduce computational effort. The second layer has a grid size of 10^{-4} m and the third layer of 10^{-3} m. There is a consecutive increase in grid size between the three layers.

The boundary condition at the end of the third layer is the ambient temperature T_U.

$$X_P = \sqrt{\frac{\kappa}{\pi f}}\ln(100) \tag{25}$$

The wall heat transfer depends on process frequency, or rather, the engine speed f. With rising engine speed, the penetration depth is lower and therefore the amount of heat transferred between liquid and wall decreases. The penetration depths of the used materials are given in Table 1.

Fig. 9 shows the influence of different wall materials on wall heat transfer in the given simulation conditions. By taking wall heat transfer into account, isentropic efficiency decreases with increasing thermal diffusivity (thermal properties given by Table 1). For each first layer material, the layer configurations have been varied whereby the first layer defines the whole influence on the isentropic efficiency and the second and third layer have almost no influence. This proves the assumption that the transient heat transfer only takes place within the penetration depth, which is equal to the first layer in our calculation. When using a thermal insulating cyclone material, PTFE and PEEK for instance, the impact of wall heat transfer on the isentropic efficiency is negligible.

5. Isentropic efficiency of the expansion unit

This chapter presents simulation results for the isentropic efficiency of the expansion unit in relation to the injection temperatures T_I and the expansion end-temperature T_E as well as to engine speed and stroke volume.

The simulation conditions are the same as in Section 4 ($\gamma = 1$; $\varepsilon_{max} = 3$; $\zeta = 6$; $\phi_L = 0.25$; $a_C = 200{,}000$ m/s^2; $\beta = 60°$; $p_{I,min} = 3$ MPa). As the impact on isentropic efficiency of using a thermal insulating material for wall heat transfer is small and the computational effort is massive, the cyclone wall is considered to be adiabatic. Furthermore we assume an efficient alternation of load where residual additional mass is considered to be zero. Mechanical losses are considered by the overall constant factor 0.9.

5.1. Impact of temperature

The results for the isentropic efficiency in relation to injection temperature T_I for different working fluids are presented in Fig. 10. For each working fluid three curves are plotted showing different expansion end-temperatures T_E. With decreasing expansion end-temperature the injection mass decreases and the resulting isentropic efficiency increases. A lower injection mass results in a smaller dead volume and a faster injection time period. Furthermore, by comparing the different working fluids, a higher vapor density at expansion end-temperature leads to a higher injection mass and the isentropic efficiency decreases. For instance at an expansion end-temperature of 303.15K the vapor density of water is 0.0512 kg/m^3 compared with 0.3219 kg/m^3 for ethanol and 4.4586 kg/m^3 for i-pentane.

For constant expansion end-temperature we determine an increasing isentropic efficiency by decreasing injection temperature. This conflicts with the finding that isentropic efficiency decreases with increasing injection mass because the injection mass and the isentropic efficiency both increase. Thus, it has to be taken into account that the phenomenon of spontaneous evaporation within the dead volume is greater in higher temperatures because of higher exergy. Hence, a higher injection temperature creates an increased exergy loss due to dead volume.

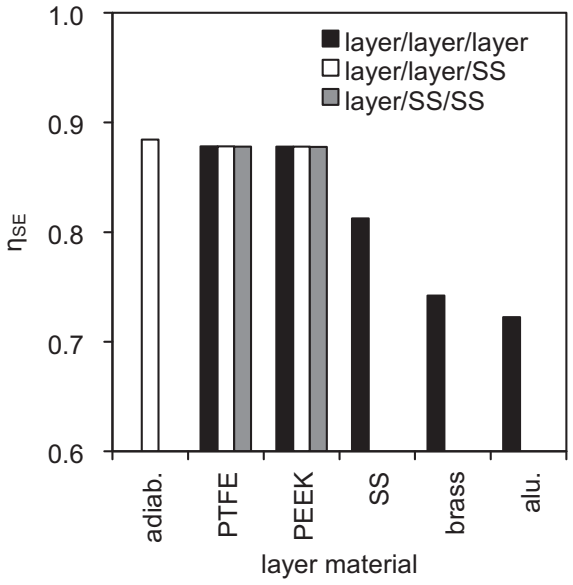

Fig. 9. Isentropic efficiency in dependence of different cyclone wall materials (first layer) for different layer configurations; $T_I = 473.15$ K, $T_E = 373.15$ K; $f = 10$; $\delta = 4.2$.

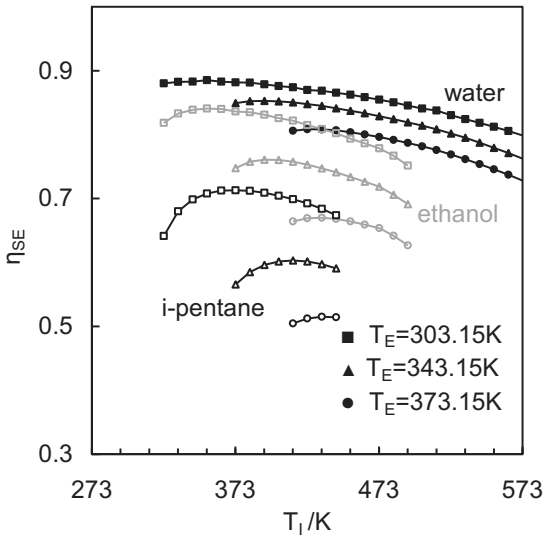

Fig. 10. Isentropic efficiency in dependence of the injection temperature T_I for different expansion end-temperatures T_E and working fluids.

It should be noted that isentropic efficiency is only one parameter in the determination of the power output of the expansion unit as shown by Equation (1). Beside the specific work l_E of the expansion unit, and the engine speed f, the power output increases proportional to the injection mass. The power output may increase for comparable stroke volume and engine speed, although the isentropic efficiency will decrease for working fluids with higher injection mass.

5.2. Impact of engine speed and stroke volume

The isentropic efficiency of the expansion unit is simulated for constant injection temperature and expansion end-temperature in relation to engine speed and stroke volume. Fig. 11 shows the results of three different working fluids. In the case of water we chose 473.15K as injection temperature T_I and 373.15K as expansion end-temperature T_E. Using ethanol T_I is 453.15K and T_E 353.15K and i-pentane was used between 403.15K and 303.15K. The expansion end-temperature was chosen so that the saturation pressure at the end of expansion is close to ambient pressure. This is not a requirement for the process, but makes it easier to handle, because the discharge of vapor takes place at ambient pressure. In order to gain a high output of specific work, the injection temperature was chosen 100K above the expansion end-temperature, whilst still avoiding the critical point.

The simulation results presented in Fig. 11 show that isentropic efficiency for small stroke volumes is not greatly influenced by engine speed. With increased stroke volume, the isentropic efficiency decreases faster at higher engine speed. This is because of increased injection mass due to increased stroke volume, and also because of an accompanying increase in injection time ratio. While the dead volume ratio δ is constant the reduction of isentropic efficiency is only attributed to the injection valve performance.

In order to efficiently use large amounts of low temperature heat, multiple parallel cyclones could be used with one cylinder instead of scaling up the unit.

For a given engine speed, injection temperature and mass flow, the expansion unit should have specially defined properties for operating at the top efficiency. A change in mass flow can easily be dealt with using multiple parallel units, where only the necessary units are operating. If either the heat source or the injection temperature (or both) is changed for an available expansion unit and fixed engine speed, there are two possible ways to address load control. On one hand, the cyclone geometry needs to be designed for the lowest expected injection temperature, which is equal to the highest injection mass. Therefore, the dead volume will be higher than necessary for higher injection temperatures. On the other hand, the expansion end temperature can be adapted to have a constant injection mass. For higher injection temperatures, the expansion end temperature needs to be increased but for lower values the expansion end temperature, and therefore the condensation level, needs to be decreased and this might not be always possible.

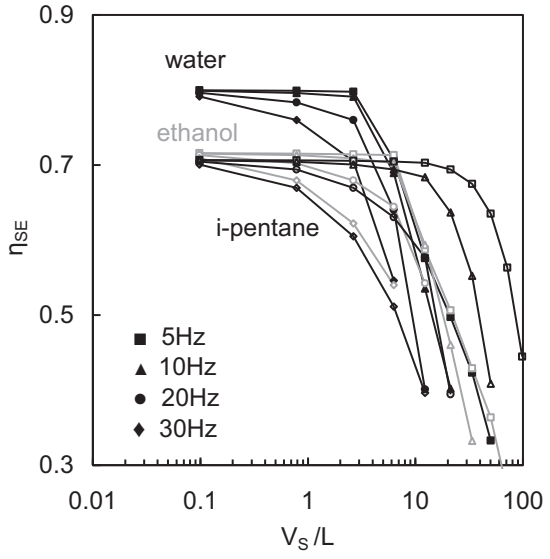

Fig. 11. Isentropic efficiency in dependence of the piston engine stroke volume for different engine speeds and working fluids.

6. Triangle Cycle efficiency and comparison with ORCs

The isentropic efficiency of the Triangle Cycle expansion unit has been presented in Section 5 in respect of temperature and engine speed as well as of the stroke volume of the piston engine. To compare the Triangle Cycle with common cycles for utilization of low temperature heat, the Organic Rankine Cycle for instance, we will have a look at the entire process, including the external heat exchanger, the condenser and the pump. Each unit has a certain impact on the exergy loss that becomes noticeable when looking at the exergy efficiency of each cycle.

6.1. The Organic Rankine Cycle

An initial comparison of a Triangle Cycles with ORC was carried out by Fischer [4]. Fischer [4] made detailed calculations for comparing Triangle Cycles and the ORCs, including pinch point analysis within the heat exchanger. He used the same isentropic efficiency for the expansion units of the Triangle Cycle as for the ORC turbine ($\eta_{ST} = \eta_{SE} = 0.85$). He also set the boundary conditions regarding the temperature level to the inlet temperature of the heat source and coolant for five different inlet temperature combinations. The working fluid and process conditions of the ORCs have been optimized to the particular temperature conditions. In some cases supercritical ORCs have been mentioned. In the case of the Triangle Cycle only water has been investigated as working fluid. Fischer assumed the isobaric line of the heat source to be linear.

6.2. Basic assumptions for process evaluation and comparison

In this study we use the inlet temperature of the heat source and the coolant as boundary conditions, whereas a constant inlet temperature of the coolant is used and the heat source temperature is varied between 333.15K and 573.15K. Furthermore, the isentropic efficiency of the expansion unit of the Triangle Cycle is set individually for each working fluid, as was stated in Section 5. It becomes clear that the isentropic efficiency used by Fischer [4] for the expansion unit of the Triangle Cycle is quite high, when considering working fluids other than water. The isentropic efficiency of the ORC turbine used by Fischer [4] seems also to be very high. Large turbines in the scale of 1 MW and optimized engine operation point might reach values of 0.85 but in smaller scales of turbine size [30] or deviated from operation point [31] the isentropic efficiency might be less. Nevertheless, in order to keep the studies comparable, we used 0.85 for ORC turbine efficiency and 0.65 for the pumps.

In this study, different working fluids for the Triangle Cycle are investigated and an optimization regarding the injection temperature of the expansion unit is performed.

Within the external heat exchanger (EHE) the heat from the heat source is transferred to the working fluid of the related process. The ORC external heat exchanger is a heater and evaporator which is

expected to have a high exergy loss. The Triangle Cycle external heat exchanger is a liquid–liquid heat exchanger. For the ORC evaporator a minimum temperature difference of 10 K is used and for the Triangle Cycle liquid–liquid heat exchanger a minimum temperature difference of 5 K is used. Liquid water with a pressure 10% above the saturation pressure of the inlet temperature T_5 (see Fig. 1) was used as a heat source. The outlet temperature T_6 is optimized to have a maximum power output and depends on the process and the actual conditions. Furthermore, a pinch point analysis for the EHE is performed. In order to inject only liquid into the Triangle Cycle expansion unit, a maximum injection temperature of 95% of the critical temperature is used. In ORCs at least 5K superheating of vapor is applied. If vapor quality after expansion inside the turbine is expected to be lower than 95%, then superheating is increased.

By increasing heat source temperature, a supercritical ORC might be feasible which would promise a better adaptation of the supercritical isobaric line to the heat source. In this case, a supercritical ORC is used with a working fluid pressure 20% above the critical pressure. Subcritical cycles are considered up to an evaporation temperature of 95% of the critical temperature.

Each process uses water as coolant in the condenser with an inlet temperature of $T_7 = 288.15$K, an outlet temperature of $T_8 = 301.15$K and a pressure of 0.5 MPa. The minimum temperature difference in the condenser is set to 10K for all cycles.

The ORC exergetic efficiency is not improved by using an internal heat exchanger (IHE) because it only reduces the amount of heat from the heat source and the heat source end temperature T_6 rises. Furthermore the coolant mass flow decreases. But the exergy of the heat source, as well as the power output of the turbine, stays unchanged. IHE was not considered in the case of ORC simulations.

6.3. Simulation results

In Fig. 12, exergetic efficiency in relation to the heat source temperature is presented for different working fluids for Triangle Cycles and Organic Rankine Cycles.

For each cycle and working fluid a maximum exergetic efficiency can be determined. In the case of Triangle Cycle and subcritical ORC the maximum point is reached when the injection temperature $T_I = T_3$ (see Fig. 1) cannot be increased, even though the heat source temperature is increased, because of the limitation of the critical point ($T_3 \leq 0.95\ T_{crit.}$). For supercritical ORC, a strong increase in exergetic efficiency, prior to reaching the maximum point, is achieved by increasing the heat source temperature. This is attributed to the supercritical pressure curve of the ORC, which is much more suited to the isobaric line of the heat source. Therefore, the exergy losses of the external heat exchanger are reduced significantly. Isentropic efficiency slightly decreases beyond the optimum point, because of increasing exergy losses in the EHE for a constant pressure of the working fluid ($p_3 \leq 1.2\ p_{crit}$) and an increasing heat source temperature.

Up to a heat source temperature of 453.15K Triangle Cycles with working fluids water, ethanol and c-pentane show the highest exergetic efficiencies (see Fig. 12). For ORC we also considered n-butane as proposed by Fischer [4], but this is not shown in Fig. 12. The exergetic efficiency of the best Triangle Cycle (water at 393.15K: $\eta_{Ex} = 43.34\%$; water at 453.15K: $\eta_{Ex} = 57.17\%$) is between 35% and 70% higher than for the best ORC (supercritical propane at 393.15K: $\eta_{Ex} = 25.16\%$; supercritical propane at 453.15K: $\eta_{Ex} = 42.12\%$).

At higher heat source temperatures the exergetic efficiencies of Triangle Cycles (water at 493.15K: $\eta_{Ex} = 61.16\%$; water at 553.15K: $\eta_{Ex} = 62.90\%$) are slightly higher (3% and 10%) than of the supercritical ORCs (supercritical i-pentane at 493.15K: $\eta_{Ex} = 55.49\%$; supercritical c-pentane at 533.15K: $\eta_{Ex} = 60.96\%$). When limited to the subcritical ORCs we determine the advantage of the Triangle Cycle to be 10%–25% (i-pentane at 493.15K: $\eta_{Ex} = 48.80\%$; c-pentane at 533.15K: $\eta_{Ex} = 55.00\%$).

It must be noted that the Triangle Cycle is calculated with a realistic isentropic efficiency over the entire temperature range, which is quite low for working fluids with high injection mass. For ORCs a quite high isentropic efficiency is used and remains constant over the mentioned temperature range.

When considering processes in term of their exergetic efficiency, it is important to correctly identify the optimum working fluid for each given heat source temperature, the state in which the cycle operates (sub-, supercritical, limitation due to critical temperature) and to know the heat exchanger pinch point. We therefore plotted an example $T, \Delta\dot{H}/\dot{Q}23$ diagram to visualize the pinch points and cycle conditions for four different working fluids and the heat source temperature 453K. Fig. 13 shows the result for the

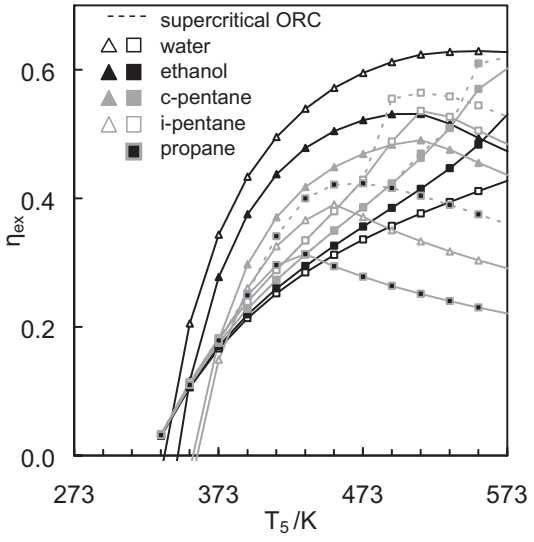

Fig. 12. Exergetic efficiency in dependence of the heat source temperature T_5 using Triangle Cycle (Δ) and ORC (□) for different working fluids.

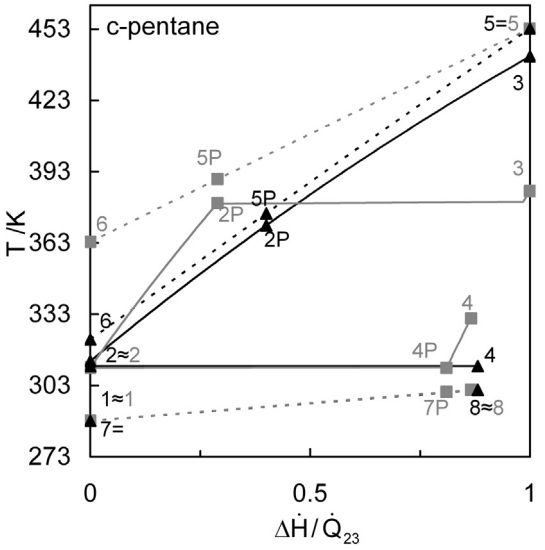

Fig. 13. $T, \Delta\dot{H}/\dot{Q}23$ Diagram for visualization of the transferred heat and pinch point analysis using Triangle Cycle (Δ) and ORC (□); $T_5 = 453.15$K; working fluid: c-pentane.

working fluid c-pentane. For the Triangle Cycle we calculated the pinch point of the EHE at the point 2P, which is somewhere between the inlet and outlet points of the EHE. In the case of the ORC the pinch point 2P is equal to the boiling point temperature of the subcritical isobaric line. Caused by the different pinch points the heat source outlet temperature T_6 is different and with almost 40K difference considerably higher for ORC. The resulting exergetic efficiencies of Triangle Cycle is with 44.86% compared with 34.96% of ORC about 28% higher, although the isentropic efficiency of the Triangle Cycle expansion unit is 74% compared to 85% for the ORC turbine. In Fig. 14 the $T, \Delta\dot{H}/\dot{Q}23$diagram for the supercritical ORC with propane and for the Triangle Cycle with water are plotted. In case of the Triangle Cycle, we can determine the pinch point at state point 2 and a good fit between the isobaric line of the heat source and the working fluid. The ORC mentioned here is supercritical and, when compared to c-pentane (see Fig. 13), the gap between the supercritical pressure curve and the isobaric line of the heat source is decreased, but is still higher than that of water in case of the Triangle Cycle.

In Fig. 15 the exergy losses for Triangle Cycles and ORCs are compared using different working fluids in the same simulation conditions as previously mentioned ($T_5 = 453$K). The exergy losses are related to the total exergy of the heat source. In all cases the exergy loss in the pump is low, even for high-pressure cycles such as supercritical ORCs. Due to the better fit of the Triangle Cycle isobaric line to the heat source, the exergy losses within the EHE are lower than all those of the ORCs. The exergy losses within the expansion unit are related to isentropic efficiency. Therefore, the exergy losses for the Triangle Cycles with the mentioned working fluids c-pentane and i-pentane are much higher than those of water or of all ORCs. Within the condenser the exergy losses are similar due to the constant coolant conditions. Differences are caused by slightly different coolant mass flows and inlet temperatures of working fluid into the condenser. The values “heat out” and “cool out” mean the outlet flows of heat source and coolant. Their temperatures are above ambient temperature and therefore, their exergy is lost. In case of the Triangle Cycle, the heat source outlet temperature is low and therefore the exergy loss is less than in cases with high outlet temperature, such as subcritical ORCs. All exergy, which is not lost, is attributed to the turbine or expansion unit power reduced by the power of the pump. Here, power is equal

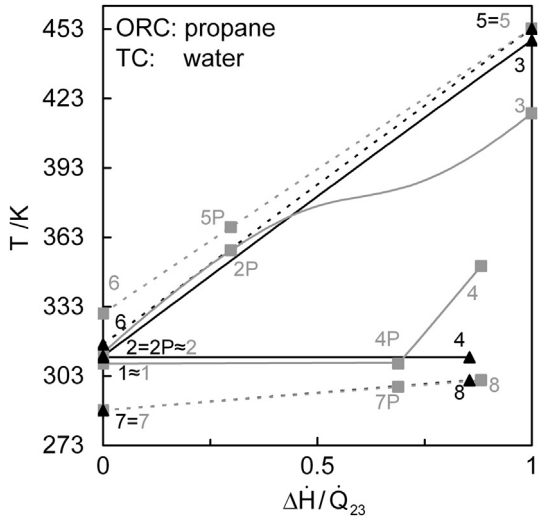

Fig. 14. $T, \Delta\dot{H}/\dot{Q}23$ Diagram for visualization of the transferred heat and pinch point analysis using Triangle Cycle with water (Δ) and ORC with propane (□); $T_5 = 453.15$ K.

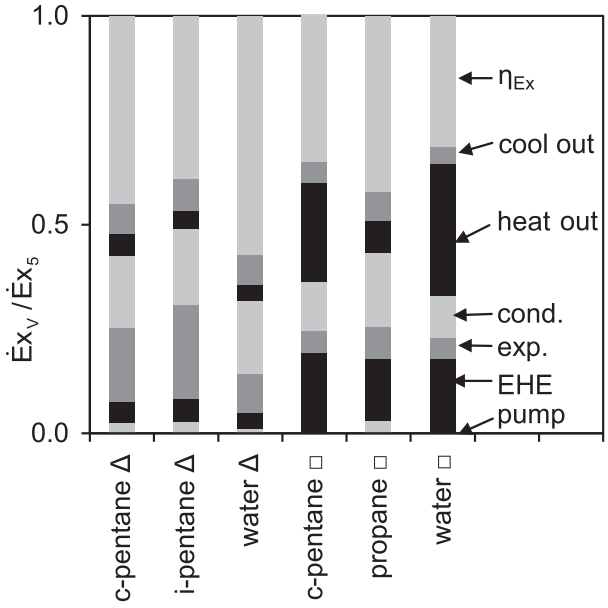

Fig. 15. Split-up of the exergy losses within the Triangle Cycle and ORC for different working fluids; $T_5 = 453.15$ K

to exergetic efficiency when dividing by the exergy of the heat source.

Beside the expansion unit and condenser, all mentioned exergy losses, especially in the EHE and remaining heat of the heat source, are considerable lower for Triangle Cycles than for ORCs.

7. Summary and conclusions

The Triangle Cycle presented here is based on the use of a piston engine as an expansion unit. Different impacts have been taken into account to calculate the isentropic efficiency of the expansion unit. The influences of dead volume, residual mass, the performance of the liquid injection and the transient wall heat transfer have been worked out. Mechanical losses are taken into account by a constant factor of 0.9. Design rules for the cyclone and injection pipe have been presented and are valid for a wide range of working fluids and their respective conditions.

It has been found that the influence of the residual mass is tremendous but can be reduced by an effective phase separation and alternation of load. Using thermal insulating material for the cyclone wall makes wall heat transfer negligible. Dead volume, mainly attributed to cyclone volume, strongly depends on the necessary injection mass of the respective working fluid. The impact of dead volume on the isentropic efficiency is larger for working fluids with high vapor densities at expansion end-temperature, which is equivalent to high injection mass. Furthermore, it has been found that the influence of injection timing is small if the injection start point in comparison to the engine speed is optimized and stroke volume or engine speed are not too high. With water as working fluid the isentropic efficiency is in the scale of 0.75–0.88, for ethanol 0.65 to 0.85 and with i-pentane as the working fluid we obtained 0.50 to 0.70.

Finally, we found decreasing isentropic efficiency at high stroke volume and engine speed, due to the influence of injection timing. For fast-running engines and high stroke volumes, a limited efficiency is expected.

In looking at the exergetic cycle efficiency, we compared the Triangle Cycles to the Organic Rankine Cycles. For a given heat source temperature, the exergetic efficiency is a measure for the

expected power output. Up to a heat source temperature of 453K, the Triangle Cycle using water as working fluids has 35%–70% higher exergetic efficiency than the best of ORCs studied. Using ethanol or c-pentane the exergetic efficiency is up to 40% higher even if supercritical ORCs are considered. At heat source temperatures higher than 493K and with consideration of supercritical ORCs the exergetic efficiency of both cycles is in the same order. With limitation to subcritical ORCs there is a benefit of Triangle Cycles using water or ethanol regarding exergetic efficiency up to a heat source temperature of 533K.

Acknowledgments

We gratefully acknowledge the support of the German Federal Foundation of the Environment (Deutsche Bundesstiftung Umwelt – DBU) and the German energy supplier EnBW. We would also like to thank Caroline McKoen for her dedicated language support.

References

[1] Srinivasan KK, Mago PJ, Krishnan SR. Analysis of exhaust waste heat recovery from a dual fuel low temperature combustion engine using an Organic Rankine Cycle. Energy 2010;35:2387–99.
[2] Tchanche BF, Lambrinos G, Frangoudakis A, Papadakis G. Low-grade heat conversion into power using organic Rankine cycles – a review of various applications. Renewable and Sustainable Energy Reviews 2011;15(8):3963–79.
[3] Bombarda P, Invernizzi CM, Pietro C. Heat recovery from diesel engines: a thermodynamic comparison between Kalina and ORC cycles,. Applied Thermal Engineering 2010;30:212–9.
[4] Fischer J. Comparison of trilateral cycles and organic Rankine cycles. Energy 2011;36:6208–19.
[5] Loeffler M. Kreisprozess mit Flashverdampfung im Arbeitsraum eines Kolbenmotors (cycle with flash evaporation in the working chamber of a piston engine), vol. 7. VGB PowerTech; 2007 [in German].
[6] Lai NA, Wendland M, Fischer J. Working fluids for high-temperature organic Rankine cycles. Energy 2011;36:199–211.
[7] Saleh B, Koglbauer G, Wendland M, Fischer J. Working fluids for low-temperature organic Rankine cycles. Energy 2007;32:1210–21.
[8] Schuster A, Karellas S, Aumann R. Efficiency optimization potential in supercritical Organic Rankine Cycles. Energy 2010;35:1033–9.
[9] Chen H, Goswami DY, Rahman MM, Stefanakos EK. A supercritical Rankine cycle using zeotropic mixtures working fluids for the conversion of low-grade heat into power,. Energy 2011;36:549–55.
[10] Ogriseck S. Integration of Kalina cycle in a combined heat and power plan, a case study. Applied Thermal Engineering 2009;29:2843–8.
[11] Zamfirescu C, Dincer I. Thermodynamic analysis of a novel ammonia-water trilateral Rankine cycle. Thermochimica Acta 2008;477:7–15.
[12] Kliem BP. Grundlagen des Zweiphasen-Schraubenmotors, Fundamentals of the Two-Phase Screw-Type Engine [Dissertation]. Fakultät Maschinenbau der Universität Dortmund; 2005 [in German].
[13] Kauder K, Kliem B. Zweiphasen-Schraubenmotor-Probleme des Füllungsvorgangs, Two-phase screw-type engine-problems of the filling process, Schraubenmaschinen Forschungsberichte des FG Fluidenergiemaschinen, Nr. 6, Strömung, Simulation und Dynamik; 1998 [in German].
[14] Löffler MK. Flash evaporation in cyclones. Chemical Engineering and Technology 2008;31:1062–5.
[15] Löffler M, Steffen M, Schaber K. Umsetzung einer Kolbenmaschine mit interner Flashverdampfung (realization of a piston engine with internal flash evaporation), Abschlussbericht über ein Entwicklungsprojekt, gefördert unter dem Az: 25116 – 21/0 von der Deutschen Bundesstiftung Umwelt; 2010 [in German].
[16] Grote K-H, Feldhusen J. Dubbel Taschenbuch für den Maschinenbau 22. Auflage (Dubble handbook for mechanical engineering, 22nd edn.); 2007 p. 29 [in German].
[17] NIST. Reference fluid thermodynamic and transport properties database (REFPROP): version 9.0, The National Institute of Standards and Technology (NIST).
[18] Bogacki P, Shampine LF. A 3(2) pair of Runge-Kutta formulas,. Applied Mathematics Letters 1989;2:1–9.
[19] Dormand JR, Prince PJ. A family of embedded Runge-Kutta formulae,. Journal of Computational and Applied Mathematics 1980;6:19–26.
[20] Grote K-H, Feldhusen J. Dubbel Taschenbuch für den Maschinenbau 22. Auflage (Dubble handbook for mechanical engineering, 22nd edn.); 2007. p. 3.
[21] Coelho MAZ, Medronho RA. A model for performance prediction of hydrocyclones,. Chemical Engineering Journal 2001;83:7–14.
[22] Köhler E. Verbrennungsmotoren: Motormechanik, Berechnung und Auslegung des Hubkolbenmotors (calculation and designing of a piston engine), 6. Auflage [in German].
[23] Saury D, Harmand S, Siroux M. Flash evaporation from a water pool: influence of the liquid height and of the depressurization rate. International Journal of Thermal Science 2005;44:953–65.
[24] Kakac S, Sha RK, Aung W. Handbook of single-phase convective heat transfer. New York: John Wiley & Sons; 1987.
[25] Gnielinski V. Forsch. im Ing.-Wes. 61, Nr. 4; 1995. p. 240/248.
[26] Verein Deutscher Ingenieure VDI-Gesellschaft Verfahrenstechnik und Chemieingenieurwesen (GVC), VDI-Waermeatlas, 8. Auflage; 1997 Ga, Gb [in German].
[27] Mishra P, Gupta SN. Momentum transfer in curved pipes. 1. Newtonian fluids. Industrial and Engineering Chemistry Process Design and Development 1979;18(1):130–7.
[28] Baehr HD, Stephan K. Waerme- und Stoffübertragung (heat and mass transfer), 5. Auflage, Springer; 2006. p. 212–31 [in German].
[29] Baehr HD, Stephan K. Waerme- und Stoffuebertragung (heat and mass transfer), 5. Auflage, Springer; 2006. p. 175 [in German].
[30] Energy Nexus Group. Technology characterization: steam turbines, prepared for. Washington DC: Environmental Protection Agency Climate Protection Partnership Division; 2002. p. 11.
[31] Bahadori A, Vuthaluru HB. Estimation of performance of steam turbine using a simple predictive tool. Applied Thermal Engineering 2010;30:1832–8.